Mapping the Epoch of Reionization with C+ Line Tomography

Technical Development Program

Technical Development Start date: 10/1/2012
Technical Development End date: 3/31/2016
Final Technical Report submission date: 3/22/2016

Team Leads:

James J. Bock
California Institute of Technology
jjb@astro.caltech.edu

Charles M. Bradford
Jet Propulsion Laboratory
charles.m.bradford@jpl.nasa.gov

I. Technical Development List of Participants

James Bock, Caltech
Charles Bradford, JPL
Tzu-Ching Chang, ASIAA
Asantha Cooray, UC Irvine
Abigail Crites, KISS Prize Postdoc, recently awarded NSF postdoctoral fellowship
Olivier Doré, JPL
Steve Hailey-Dunsheath, Caltech
Jonathon Hunacek, Caltech graduate student, awarded NSF graduate fellowship
Chao-Te Li, ASIAA
Mario Santos, IST-Centra
Phillip Lubin, UCSB
Hien Nguyen, JPL
Roger O'Brient, Caltech postdoc, hired as JPL technologist
Erik Shirokoff, KISS Prize Postdoc, hired as assistant professor at U. Chicago
Zachary Staniszewksi, Caltech postdoc, hired as JPL systems engineer
Bade Uzgil, U. Pennsylvania graduate student, hired as postdoc at UC Irvine

II. Executive Summary

Our KISS program has laid the theoretical foundations for probing the epoch of reionization with C+ tomography measurements, developed unique lithographed millimeter-wave spectrometer technology, and initiated a first-light C+ experiment named TIME-*Pilot*. With KISS support we have carried out the following investigations:

- Developed the case for line intensity mapping methods to study the epoch of reionization using singly ionized carbon (C+), typically the most luminous emission line in galaxies. The theoretical studies not only explored the amplitude of the signal, and the usefulness in determining physical properties of the partially ionized intergalactic medium, but also the effects of foreground confusion from low-redshift galaxies. Our team made the first calculations of C+ clustering fluctuations from the reionization epoch, and estimated the effect of foreground galaxy confusion, largely from CO line emission at $z \sim 1$. We also authored the first papers on tomographic measurements with the Lyα emission line, which shows great promise for near-infrared intensity mapping measurements with the SPHEREx SMEX mission concept.
- Developed a complete design for a first-detection instrument of [CII] large-scale clustering emission named TIME-Pilot, based on an array of 32 novel waveguide spectrometers. The spectrometers are mounted in a linear array in two polarizations, and observations are carried out by scanning the detectors in a 1-deg linear strip, which maximizes depth (small survey area) while preserving sensitivity on large scales (long scan length).
- Demonstrated the key waveguide spectrometer technology, which confines radiation in 2 dimensions and the power propagates between parallel plates and is dispersed and collimated by a curved grating. The waveguide spectrometers greatly reduce the mass and volume that would otherwise be required with a conventional 3-d grating spectrometer.

- Demonstrated a prototype superconducting detector array. These high-sensitivity superconducting bolometers are mounted on the focal surface across multiple spectrometers, and read out by superconducting current amplifiers. The devices present unique micro-machining challenges to produce edge-butted sub-arrays that do not leave spectral gaps between channels.
- Completed the full cryogenic system for the instrument. We commandeered an existing 4 K cryostat from another project, and added cooling stages to an ultimate temperature of 220 mK to meet the TIME-Pilot cooling requirements. The system is fully tested and operational.
- Formed a partnership with ASIAA in Taiwan, led by Tzu-Ching Chang who attended the original KISS study. ASIAA is providing major hardware components for the TIME-Pilot instrument, and in the past year have developed a prototype of the spectrometer, and procured cables and cryogenic coolers. ASIAA has also become the managing institution for the James Clerk Maxwell Telescope (JCMT) in Hawaii, and ideal facility for carrying out observations with the instrument.

III. Introduction

Role of the KISS First Billion Years Study

Our KISS technical development program began with *The First Billion Years* KISS study exploring new methods to probe the epoch of reionization (EoR) when the first stars and galaxies formed. The study resulted in an important new finding, that large-scale maps of galactic emission lines would be a valuable counterpart to the current program of HI experiments.

Currently several large experiments are being fielded (e.g., PAPER, MWA, LOFAR) that map HI from the EoR, tracing the neutral hydrogen in the intergalactic medium before it is ionized by UV radiation from the first stars. In contrast, emission line mapping reveals the underlying distribution of galaxies, which trace the ionized regions. The combination of emission line measurements with HI provide additional information about the EoR process, and are sensitive to the history of the ionization and the history of the characteristic 'bubble size' of ionized regions. The line mapping instruments would use a new method called "intensity mapping", mapping large scale structures associated with large-scale galaxy clustering without resolving the individual galaxies.

The galactic emission line measurements are complementary to HI measurements also in that systematic errors and contaminating foregrounds are much different, leading to robust cross-comparisons. The study identified 3 promising emission lines for observational exploitation, carbon monoxide (CO) redshifted to the radio, ionized carbon (C+) redshifted into the millimeter-wave, and Hydrogen (Lyα) redshifted into the optical.

Intensity Mapping the Epoch of Reionization

The EoR is the first chapter in the history of galaxies and heavy elements, marked by the onset of the first generation of stars. During the period between 200 Myr and 1 Gyr after the Big Bang ($6 < z < 20$), the first baryonic objects collapsed in dark matter halos, ignited the first stars, and produced enough Lyman-continuum photons ($h\nu > 13.6$ eV) to reionize the surrounding hydrogen gas. The very first stars were likely metal free and short-lived, ending in supernovae that enriched the cosmos with the first heavy elements. Subsequent generations of stars then fully reionized the intergalactic medium

(IGM). Detecting the primordial galaxies responsible for reionization individually is difficult as they are intrinsically low-mass, low-luminosity objects.

For example, Wise et al. 2014 find that the typical reionizing photon comes from a L ~ 10^9 $L_\odot$, 10^8 $L_\odot$, 10^7 $L_\odot$ galaxy at z = 6, 8 and 10, respectively. Extremely deep imaging with HST has begun to probe the very bright end of the UV luminosity functions at z > 6, but the faint-end slopes are poorly constrained, and at the highest redshifts the total light integrals diverge (see Fig. 1). Observing lensed fields (e.g. the HST Frontier Fields) may offer a factor of 10 improvement, and JWST will also offer on order 10× improvement over HST later in the decade. But at best these new measurements will still reach to only L ~ 3 × 10^8 $L_\odot$ at z=8, leaving undetected the sources that produce the majority of ionizing photons. Similarly, ALMA can offer individual detections of the most luminous individual sources in the submillimeter (in [CII] and/or dust), but even in a prohibitively long (1000-hour) integration, ALMA at z~7–8 will be sensitive only to ~1×10^6 $L_\odot$ in [CII], equivalent to a ~3×10^8 $L_\odot$ galaxy (assuming dual pol sensitivity, 3σ detection, 200 km/s linewidth, scaled from 0.084 mJy 1 sigma, 1 hour, at 237 GHz).

Intensity mapping traces emission from large-scale linear galaxy clustering, which measures the total bolometric light production integrated over all galaxy populations. 2-D intensity mapping studies have been quite successful in measurements of the CMB, which constrain the EoR epoch through measurements of optical depth and patchy reionization. Recently, continuum intensity mapping has been used to study the linear and non-linear clustering of sub-mm galaxies, trace the large-scale structure that gravitationally lenses the CMB, and to discover a new component of the near-infrared extragalactic background. While these 2-D studies demonstrate the basic technique, broad spectral bands integrate emission over redshift. Spectral measurements incorporate 3-D redshift information needed to distinguish the faint EoR signal from the bright low-redshift galaxies along the line of sight.

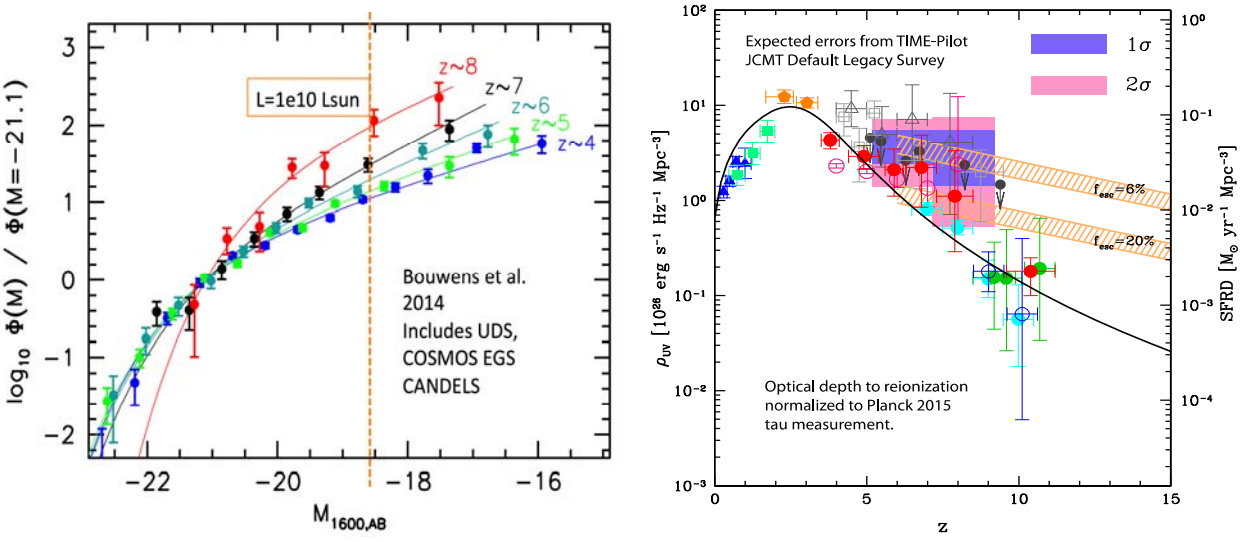

Figure 1. Star formation and galaxy populations in the Epoch of Reionization. *Left*: luminosity functions measured with via deep dropout surveys with Hubble; faint-end slopes are steep and the total integrals do not converge for the highest redshifts, which indicates that the galaxies producing the bulk of the EoR photons lie below the detection limit. *Right*: Star formation rate density (SFRD ~photon production density) history as measured with (heavily extrapolated) galaxy counts (points) and as required to match the Planck tau (orange hatched) under two escape fraction (f_{esc}) assumptions (adapted from Robertson et al, 2015). TIME-Pilot offers an independent way to measure the SFRD via intensity mapping of [CII]. 1 & 2 sigma sensitivities refer to 67% and 95% confidence about the f_{esc}=6% model, assuming a 240 hour survey at the JCMT, and $L_{[CII]}$ / L_{tot}= 3x10^{-3}.

3-D intensity mapping uses an imaging spectrometer to measure a spatial-spectral data cube in which intensity is mapped as a function of the sky position and frequency. This data cube is then analyzed to produce a 3-D power spectrum. The first 3-D intensity mapping measurement detected 21-cm fluctuations in a GBT HI survey at $z \sim 0.9$. Other HI experiments as well as CO intensity mapping experiments, with first limits on the CO abundance at $z \sim 2$ to 3, are now underway, probing various cosmic epochs including the EoR and later times.

With KISS support, we developed a new millimeter-wave imaging spectrometer concept named TIME-*Pilot,* which targets the [CII] emission from ionizing galaxy populations. TIME-*Pilot* will map the 3-D [CII] intensity power spectrum to reveal the linear clustering signal and thereby constrain EoR photon production, as illustrated in Fig. 1. [CII] is the most energetic emission line in galaxies for $\lambda_{rest} > 40$ μm, and is a bolometric marker for total star formation activity (see Fig. 2). TIME-*Pilot* traces the integrated star-formation rate density by measuring the aggregate [CII] intensity of proto-galaxies responsible for reionization. [CII] complements HI 21-cm line intensity mapping that traces the neutral medium at $z > 6$. Given a first detection of [CII] fluctuations, a future generation of instruments will make full [CII] data cubes that can be cross-correlated with HI data to trace the bubble size and ionization history of the intergalactic medium.

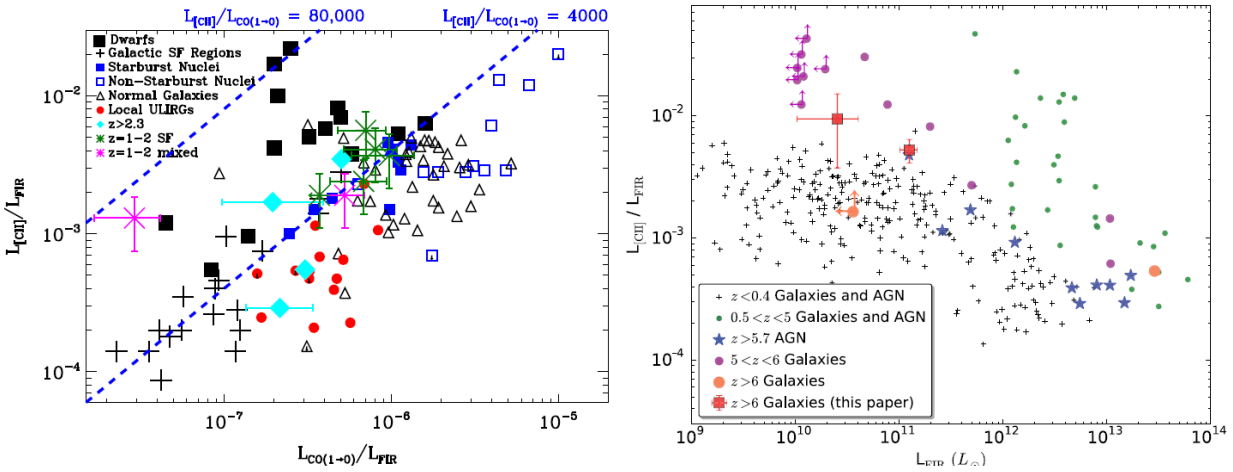

Figure 2: *Left:* [CII] emission as a function of CO emission for a range of galaxies and Galactic regions from Madden et al. (2013), adapted from Stacey et al., 2010. Low-metallicity dwarf galaxies which are likely analogs of the EoR systems lie in the upper left corner of this plot, with both enhanced [CII] and suppressed CO. (The 50 Herschel DGS galaxies are not yet available, but Madden et al. report [CII] to far-IR ratios is 0.005 to 0.02). *Right:* Recent compilation of high-z [CII] measurements from Willott et al. (2015), (including the Capak et al. (2015) galaxies) showing that [CII]-to-bolometric luminosity ratios are typically in excess of 10^{-3} in high-redshift galaxies, particularly when AGN are excluded and for $L<10^{11.5}$ $L_{\odot}$, as expected for the EoR population.

a. Why Study Ionized Carbon Emission?

Carbon is the fourth-most abundant element in the Universe and, with an 11.3 eV ionization energy that is less than that of hydrogen (13.6 eV), is easily ionized by diffuse starlight. With a fine-structure level splitting of 91 K, and modest critical densities in both neutral and ionized gas, [CII] is easily excited and radiates efficiently at 157.7 μm. Conveniently, [CII] is redshifted into the relatively transparent 1 mm atmospheric window (195–310 GHz) for $5 < z < 9$, the

target band for TIME-*Pilot*. [CII] provides a major cooling mechanism for the interstellar medium (ISM), in multiple phases of the ISM in the Galaxy, including diffuse regions. As a result, the [CII] line is among the brightest of spectral lines in the aggregate spectra of star-forming galaxies, accounting for 0.1% to 1% of the total IR luminosity, and has been detected in high-redshift galaxies.

With the advent of ALMA, [CII] is now being studied (and discovered serendipitously) in $z > 4$ galaxies. We highlight a recent survey of ten $z \sim 5$–6 Lyman-break galaxies (LBGs) in the continuum and [CII] with ALMA (Capak et al., 2015). [CII] is robustly detected in all 10, even though the continuum is only detected in 4 of the 10. The authors find that the dust is depleted relative to that expected from the UV spectral slopes calibrated at lower redshift, but as Fig. 2 shows, the [CII] to far-IR bolometric ratio is as high or higher than that in local galaxies ($\sim$0.1-1% below $L \sim 10^{12}$ $L_\odot$, and trending higher for low-luminosity systems overall). They find that [CII] serves as an excellent total star-formation-rate (SFR) tracer, when both UV and far-IR luminosities are included in estimating the SFR.

Spectral intensity mapping is also pursued using redshifted CO, including an upper limit at $z \sim 2$ to 3. We emphasize that [CII] is typically 4000 times more luminous than CO J=1→0 in local galaxies. The ratio will likely be even higher for the EoR systems since they are believed to resemble the local low-metalicity dwarf galaxies, for which [CII] is enhanced with respect to both total far-IR emission and CO emission (see Figure 2, left).

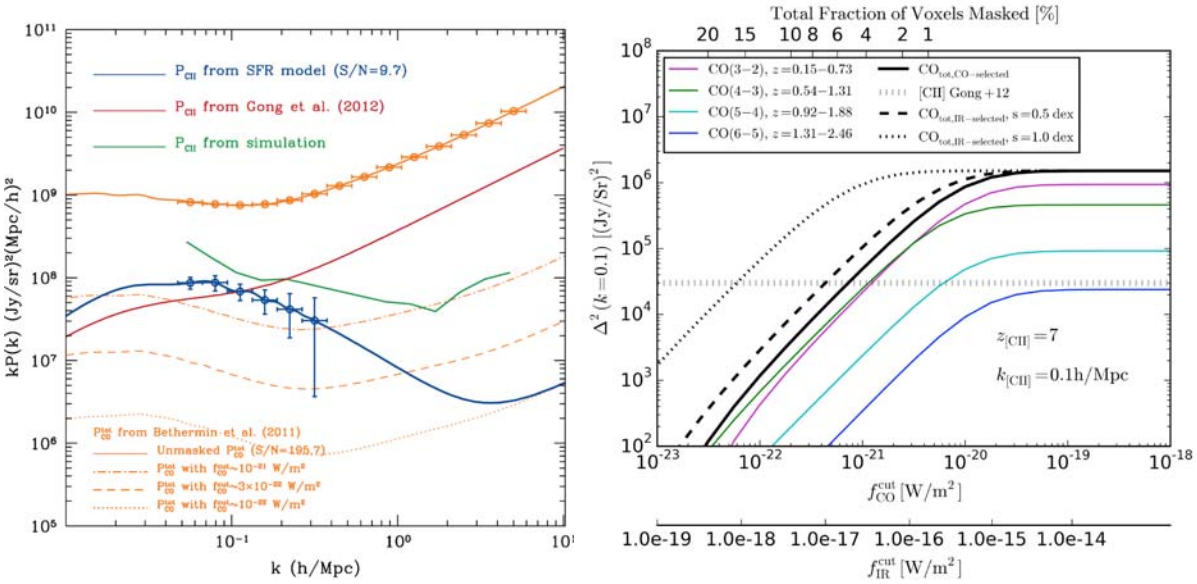

Figure 3: *Left:* 3-D power spectra (in $kP(k)$ units) of EoR [CII] and intermediate-z CO in the TIME-Pilot band. Red, blue, and green curves mark [CII] power from the 'Gong high,' 'SFR', and 'Silva simulation' estimates, respectively, described in the text. The orange lines show power in CO: the upper curve includes all the CO-emitting galaxies, the lower broken curves show the power after masking to various depths. CO signals are cast in the [CII] k-space to enable direct comparison. *Right*: CO masking requirements. The horizontal dotted line is the expected [CII] power spectrum amplitude at k = 0.1 Mpc^{-1}. The curves show the estimated amplitude at the same k (k[CII] = 0.1 Mpc^{-1}) produced by CO in intermediate redshift galaxies as a function of the masking cut. The heavy black curves show the signal from all CO transitions combined. The dashed and dotted include the effect of selecting based on IR flux instead of CO and refer to the lower f^{cut}_{IR} axis, which requires deeper masking because of the scatter in the CO to IR luminosity relation (see text). We show conservatively large scatters of 0.5 and 1 dex. All black heavy curves refer to the upper axis showing the fraction of TIME-*Pilot* voxels which must be masked. For reference, a FIR flux of 10^{-17} W m^{-2} corresponds to $\log(L/L_\odot)$ = 9.40, 10.14, 10.58, 10.89 at z = 0.5, 1.0, 1.5, and 2.0, respectively.

b. Prospects for [CII] Detection

We have studied the prospects for detecting large-scale linear [CII] clustering with a wide-band imaging spectrometer. We first computed the expected EoR [CII] intensity as a function of redshift and found a reasonable agreement when using three different approaches, shown in Figure 3. First, the 'High' Gong et al. (2012) case is based on a first-principles gas physics excitation analysis, painted onto semi-analytical galaxy formation models. Next, the 'SFR' case assumes an estimated high-z star formation rate and a fixed [CII] to bolometric emission ratio of 2×10^{-3}, and partitions this mean intensity into a galaxy luminosity function which incorporates models for large-scale structure. Third, the 'Simulation' Silva et al. (2014) case applies a [CII] to bolometric ratio based on a recent fit to high redshift galaxies by De Looze et al. (2014) into the De Lucia et al. (2006) galaxy catalogs based on the Millennium simulation.

Fig. 3 shows the sensitivity of our proposed instrument TIME-*Pilot* in 240 hours on sky compared with theoretical [CII] power spectra. The dominant term is the Poisson noise due to the random distribution of galaxies, but clustering becomes important on large scales. The amplitude of the small-scale 1-halo clustering term yields the typical halo mass scale of star-forming galaxies at $z > 5$. The latter is a crucial ingredient for models of galaxy formation and evolution since it establishes the halo mass scale in which gas cooled most efficiently for forming the first proto-galaxies. We find that TIME-*Pilot* can detect the linear EoR [CII] clustering amplitude that traces total light production with S/N ~10 for all 3 models.

c. CO Foreground Line Emission

TIME-*Pilot* observations will also capture the integrated CO intensity fluctuations arising from intermediate-redshift galaxies. For EOR studies, these rotational CO lines act as a foreground and must be identified and subtracted to reveal the [CII] signal. Figure 3 (right) shows the fraction of TIME-*Pilot* voxels required to mask CO emitting galaxies. In practice, we plan to mask based on IR luminosity because individual galaxy CO fluxes themselves will not be accessible. Masking estimates must thus account for the scatter between IR luminosity and CO. We begin with the latest Bethermin et al. (2011) luminosity functions and incorporate a CO / LIR prescription similar to that in Carilli & Walter (2013). Dessauges et al. find a 0.38 dex scatter in IR for a given CO flux, which corresponds to 0.3 dex scatter in CO at a given IR luminosity with their $\log L_{IR}/\log L_{CO}$ slope of 1.2.

These estimates are consistent with the recently-announced upper limit from the CO Power Spectrum Survey (COPSS) experiment. COPSS operates at 27–35 GHz, probing CO J=1→0 at z=2.3–3.3. Their limit is $P_{CO-CO} < 2.6 \times 10^4$ $(\mu K)^2 (Mpc/h)^3$ at k=1 h/Mpc. Assuming that e.g. J=6→5 has a (conservatively large) 0.3× the brightness temperature of J=1→0, this translates to 6×10^9 $(Jy\ sr^{-1})^2\ Mpc^3$ in our band, comparable to the CO variance we estimate at k=1 h/Mpc in Figure 3 (left). As Fig. 3 (right) shows, even in this model, masking to the intermediate depth of 3×10^{-22} Wm^{-2} is sufficient to render the CO power sub-dominant to the [CII] power. Even allowing for much larger scatter (assumed conservatively as 0.5 and 1.0 dex) between IR luminosity and CO, will require removing no more than 20% of the voxels.

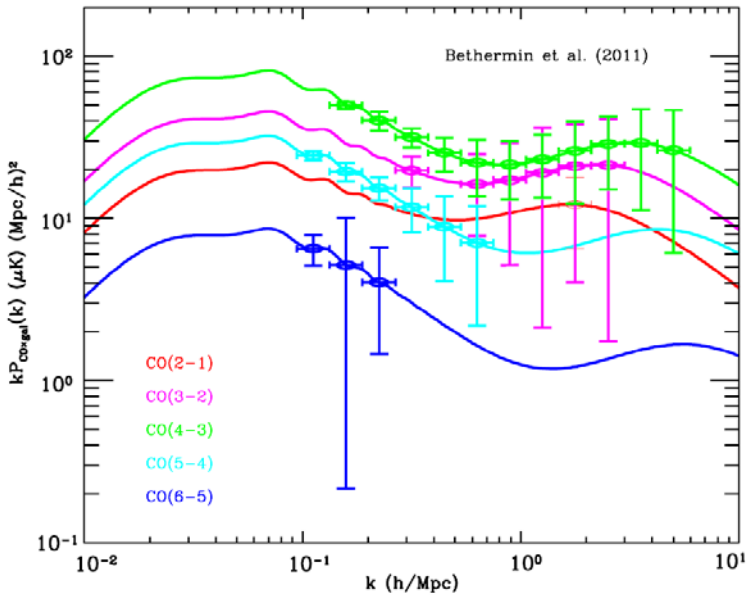

Figure 4: Cross-correlation power spectra between the various CO transitions detected in TIME-*Pilot* as part of the planned [CII] survey and the 3-D positions of z = 0−2 galaxies towards the same sky areas. We will select a field that is rich in legacy galaxy survey data, including optical and infrared spectroscopy leading to large number of redshift measurements to z of 2 (e.g. COSMOS). The cross-correlations are detected at a total signal-to-noise ratio in excess of 20 for CO J = 4→3, 15 for CO J=5→4, and 5 for CO J=3→2 and CO J=6→5.

The CO data are of interest in their own right since they provide a measure of the spatial distribution and abundance of molecular gas over a broad range of cosmic time, including the peak epoch of cosmic star formation at $z \sim 2$. Molecular gas is the fuel for star formation, a key ingredient in models of galaxy evolution. To date, most observations of molecular gas at high redshift have been restricted to galaxies selected on the basis of high star-formation rates (e.g., SFR ≥ 100 $M_\odot$ yr^{-1} at z = 0.2 − 1.0 and SFR ≥ 30 $M_\odot$ yr^{-1} at z = 1.0 − 2.5). A full census of the molecular gas content over cosmic time requires an unbiased search for CO emission with sufficient sensitivity to probe the normal star-forming galaxy population.

To optimally extract CO clustering in redshift bins, we will cross-correlate maps of individual CO transitions with existing galaxy catalogs and 21-cm tomography. Well-studied large fields such as COSMOS contain broad multi-wavelength coverage and redshift information, and these cross-correlations are readily detectable. We will stack the TIME-*Pilot* spectra on subsamples of galaxies to measure the aggregate gas properties of sources as a function of star formation rate, stellar mass, etc. A simple stacking based only on star formation rate and redshift will yield 3−5σ detections for SFR bins of 10−30 or 30−50 $M_\odot$ yr^{-1}, and narrow redshift bins centered on z = 0.5, 0.75, and 1.2 (see Fig. 4).

d. Kinetic Sunyaev-Zel'Dovich Effect Measurements

TIME-*Pilot* is ideally suited measure the kinetic Sunyaev-Zel'dovich (kSZ) effect in individual galaxy clusters. The thermal SZ (tSZ) effect has a null at 217 GHz, while the kSZ effect peaks in the TIME-*Pilot* spectral band. The kSZ effect, due to the motion of a galaxy cluster with respect to the CMB, provides a direct, redshift-independent measurement of the line of sight peculiar velocity of a galaxy cluster v_{pec}. This dynamical information can, in turn, be used to understand structure formation and virialization in clusters, cosmic acceleration, and modified gravity. Members of our team have been involved in pioneering measurements of the kSZ effect, including a spectral tSZ measurement performed with Z-Spec, which made the first detection of relativistic tSZ contributions, and the first reliable detection of the kSZ effect in an individual cluster using multiple instruments. Observations in the 200-300 GHz spectroscopic band measure the tSZ effect as it passes through the null at 217GHz, which in principle is

enough information to extract the kSZ signal (see Fig. 5). However since the tSZ effect is large, in practice highly accurate measurements of the tSZ effect are needed for a sufficiently precise separation. Therefore we have included 11 broad-band photometer channels at 150 GHz to measure the tSZ effect in the decrement. TIME-*Pilot* efficiently observes clusters using a short line scan, which keeps pixels on and off the cluster at all times.

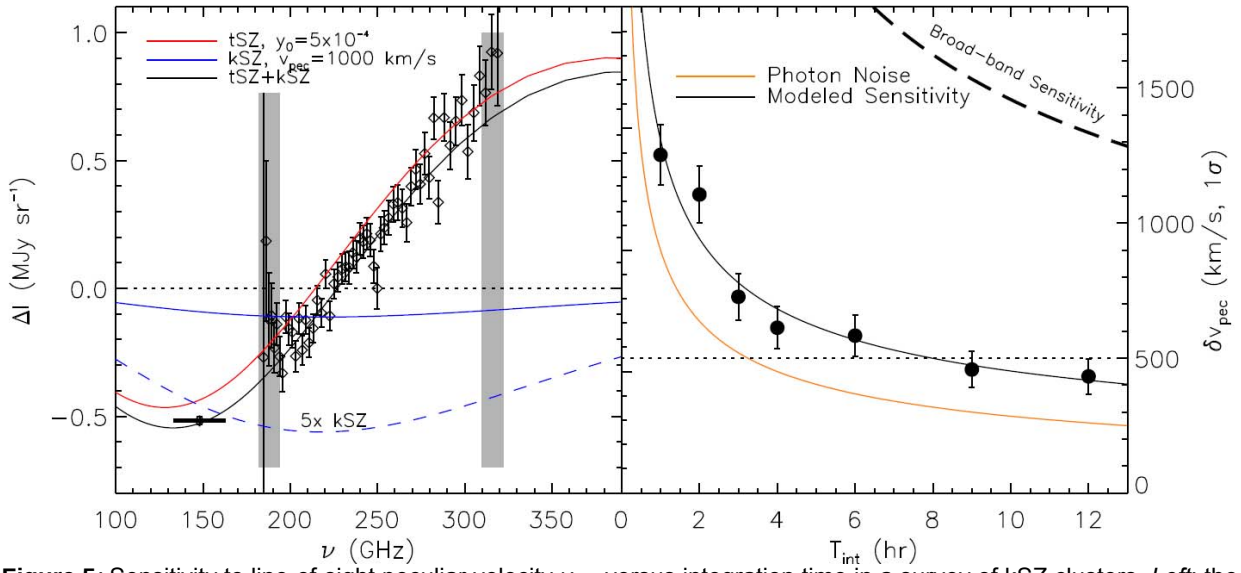

Figure 5*:* Sensitivity to line-of-sight peculiar velocity v_{pec} versus integration time in a survey of kSZ clusters. *Left*: the TIME-*Pilot* simulated measurements compared to tSZ and kSZ spectra. The atmospheric guard channels are highlighted with grey; these points are not used in the likelihood function fit to determine the best-fitting cluster parameters. The 150 GHz channel gives a longer spectral lever to help disentangle the tSZ effect from the slowly-varying kSZ signal. *Right*: simulated sensitivity to the kSZ effect including realistic astrophysical contamination and atmospheric filtering. The points show the mean uncertainty in 100 realizations of the cluster and atmospheric noise model. The estimated performance (black curve) approaches the idealized case given by the orange line, which ignores astrophysical contamination and assumes only photon noise. Broad-band kSZ measurements are strongly limited by atmospheric noise, even using an optimized spatial subtraction (dashed black line), and TIME-*Pilot* out performs them by a factor of $\sim$5 in measurement time.

Previous attempts to measure the kSZ effect have been limited by atmospheric noise. TIME-*Pilot* uses a unique atmospheric subtraction technique to gain a significant sensitivity advantage. We use atmospheric monitor channels in the wings of the broad 183 and 325 GHz water lines to regress atmospheric noise, which improves TIME-*Pilot*′s kSZ measurement speed by a factor of 5 over previous broadband experiments. We estimate our kSZ sensitivity using a detailed atmospheric noise model and simulated clusters with random CMB and CIB fluctuations. The atmospheric model is matched to measurements of broadband and spectroscopic atmospheric noise from earlier instruments on Mauna Kea. The resulting marginalized 1σ uncertainty on v_{pec} is ±500 km s^{-1} in just 8 hours as shown in Fig. 5, a major advance on current kSZ capability that enables the first cosmological kSZ surveys.

IV. Outcomes of the technical development program

a. TIME-Pilot: A First-Light Instrument Concept

TIME-*Pilot* will measure 3-D [CII] fluctuations from $5 < z < 9$ galaxies, using 32 independent single-beam, single-polarization spectrometers, as show in in Fig. 6 and Table 1, and described in detail below. The spectrometers are arrayed in two stacks of 16, one stack for each polarization. The input feeds for both stacks image to an overlapping line on the sky via a polarizing grid. Measuring the low-*k* modes sensitive to clustering (see Fig. 3) requires simultaneous wide-band spectral coverage and sensitive mapping on 10 arcminute spatial scales. The spectral bandwidth is provided naturally with our spectrometer. The deep large-scale mapping is provided by a 180x1 beam = 1.0° x 0.35′ line scan, which optimizes the S/N on the [CII] clustering amplitude. We emphasize that all TIME-*Pilot* key technologies have been demonstrated in scientific applications.

b. Novel 2D Waveguide Grating Spectrometer Technology

Instantaneous wide-band spectral coverage with background-limited sensitivity requires a grating-type spectrometer or filterbank as opposed to an FTS or Fabry-Perot. Millimeter-wave gratings once presented a technological challenge, since conventional echelle grating approaches spectrometers are too large and bulky for cryogenic operation. However, we have pioneered a unique approach using a curved grating in parallel-plate waveguide which both focuses and diffracts the broadband light from a single waveguide mode (e.g. from a feedhorn) to a detector array. This approach dramatically decreases the total volume of the spectrometer; it has been used in Z-Spec at R=250, a single-beam predecessor to TIME-*Pilot*, and in R=700 prototypes developed for 190–310 μm space and balloon applications.

Table1: TIME-Pilot Experimental Parameters.

Number of spectrometers	32: 16 each pol, grid diplexed		
Number of 150 GHz photometers	11, spectrally diplexed at $2\,f\lambda$ spacing		
Total # of detectors	1920 + 11 = 1931: TES bolometers with SQUID MUX		
Instantaneous FOV	11 arcmin × 0.35 arcmin (@ spectrometer mid-band)		
Cryostat, base temperature	Existing 4K / 1K system with ^{3}He cooler at 250 mK.		
C+ Survey volume (comoving)	153 Mpc × 0.85 Mpc × 1240 Mpc deep		
C+ Survey on-sky integration time	240 hours, estimated		
kSZ $\delta v_{\rm pec}$ sensitivity	± 500 km s^{-1} per beam in 8 hours		
Instrument Parameters			
Parameter	Photometers	Grating LF Band	Grating HF Band
Spectral range [GHz]	135 – 165	183 – 230	230 – 326
Estimated end-to-end optical efficiency	0.3	0.3	0.3
# of Bolometers per sub-band	1	24 (8×3)	36 (12×3)
Atmospheric PWV monitor channels		10: 183 – 199 GHz	6: 305 – 326 GHz
$\nu/\delta\nu$ per detector	5	92 – 122	90 – 120
NEI on sky per detector [(MJy/sr)$\sqrt{\rm sec}$]	0.3	3.3 – 4.0	5.3 – 8.3
NEFD on sky per detector [mJy$\sqrt{\rm sec}$]	6	37 – 44	42 – 56
TES Bolometer Parameters			
TES safety factor (= $P_{\rm elec}$ / $P_{\rm opt}$)	3	3–5	5–8
Detector + MUX NEP [10^{-18} W Hz$^{-1/2}$]	40	9.7	13
Photon NEP [10^{-18} W Hz$^{-1/2}$]	60	14 – 17	16 – 24
Absorber size [mm]	ϕ 4.0	3.0 × 3.48	3.0 × 2.32

Each spectrometer is a simple machined, bolted aluminum assembly, requiring global tolerances of $\lambda/10$ and low surface roughness on the waveguide plates, obtained by lapping. We note that in these previous applications, we have already demonstrated operation with higher resolving power and/or tighter tolerances than required for TIME-*Pilot*. We have designed, prototyped, and begun testing a waveguide grating for TIME-*Pilot* shown in Fig. 7. It has 190 facets and provides resolving power of >150, ensuring that detector sampling exceeds the resolving power, and the longest dimension is 31 cm. The output arc is approximated by 6 linear facets, so that when the spectrometers are stacked in the two groups of 16, each stack creates 6 planes, each 3 cm×14 cm on which the 2-D detector arrays are mounted.

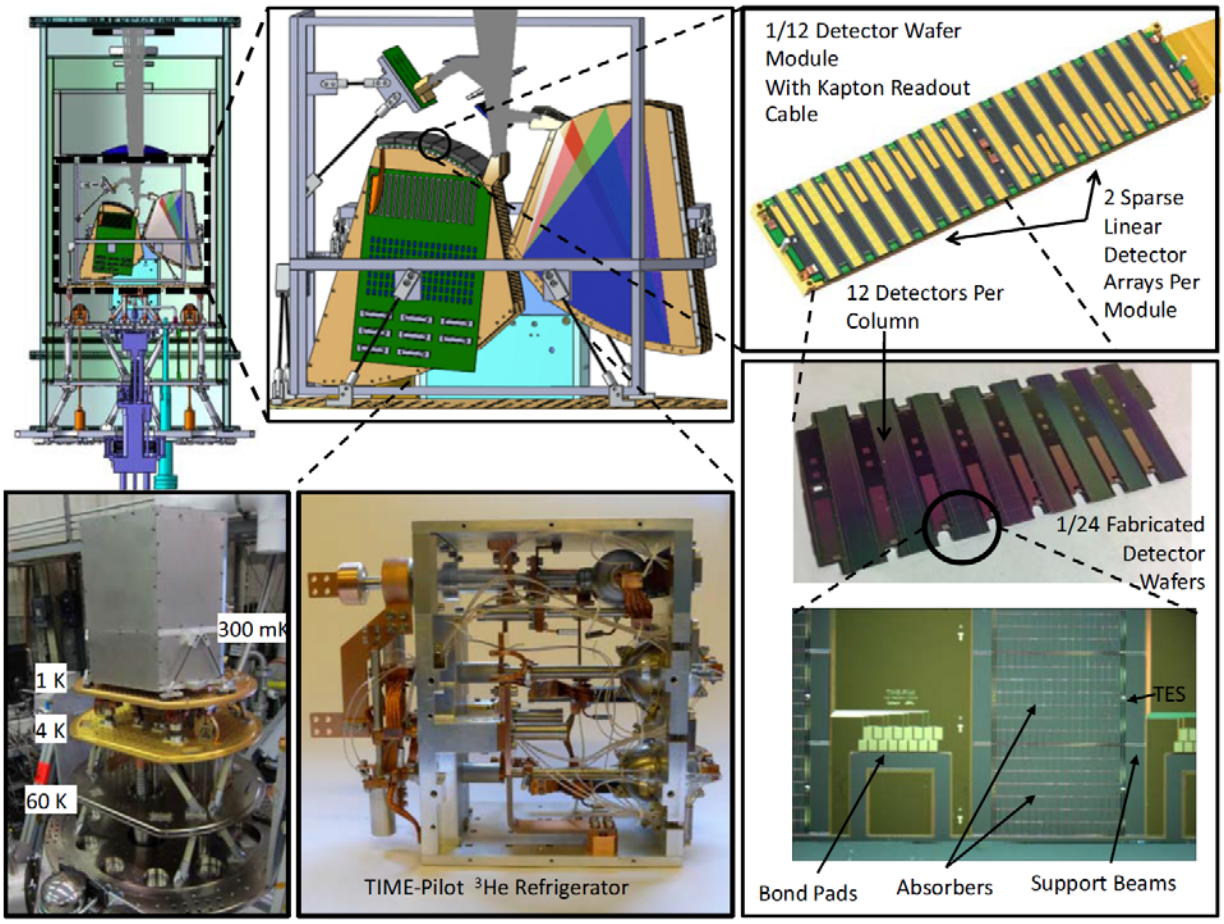

Figure 6. TIME-*Pilot* instrument overview. The instrument will be housed in an existing closed-cycle 4K–1K–300mK cryostat (bottom left), with a large cryogenic volume for the spectrometer stacks and optics (top left). 32 waveguide grating spectrometers (top center) are assembled into two stacks of 16, they couple the same 1-D linear field on the sky via an array of feedhorns and single-polarization waveguide feeds illuminated through a polarizing grid. Each grating spectrometer is similar to that used in Z-Spec, but are smaller and simpler for TIME-*Pilot* operating at lower resolving power (R=170 vs. R=250 for Z-Spec). The dispersed light is detected with twelve 2-D arrays of TES bolometers which span the spectrometer stacks (right) with a total of 1920 detectors. The TESes (lower right) are similar to those built at JPL but with mesh absorbers. A linear array of 11 150 GHz 2 $f\lambda$ channels view the same sky as the spectrometers via a dichroic filter, and will be used in surveys of the kSZ effect in galaxy clusters. The spectrometers and detectors are cooled with a custom dual-stage 250-mK / 300-mK refrigerator which has been built and tested (bottom, center).

The waveguide gratings couple to the incoming radiation by means of multi-flare-angle, direct drilled feedhorns. The full horn array is manufactured with a single custom-ground tool. Our group has successfully manufactured and demonstrated an array of similar horns, and measurements show excellent efficiency over the full frequency range (return losses $S_{11} < -20$ dB from 192−305 GHz). We have chosen to illuminate the telescope with a 10dB edge taper, which balances the desire to both couple to the sky with the best efficiency per beam, and to pack a large number of horns into the fixed field of view. With this optimized horn size, we can fit a 1×16 array of beams into the available 11′ FOV, and the spillover of each beam onto the cold stop is only ∼10%. Light from the feedhorn couples into the grating by means of a bent split-block waveguide section. The waveguide gratings are intrinsically single polarization devices, and a polarizing diplexer placed in front of the focal plane feeds two 16-element grating stacks. The waveguides in one stack include a 90° twist to align the polarization vector of the grating with that of the polarizing grid (Fig. 6).

c. TIME-Pilot at the JCMT

TIME-*Pilot* will couple to the JCMT with a modification to the SCUBA-2 relay optics. The existing mirror at the edge of the Nasmyth platform will be replaced with a larger mirror with the same optical prescription. A new mirror will be installed to intercept the beam as it travels down to SCUBA-2, and direct it up into the TIME-*Pilot* cryostat (Fig. 9). This second mirror will be mounted on a translational stage such that it may be quickly moved out of the optical path, providing rapid switching between TIME-*Pilot* and SCUBA-2 observing. The relay optics form an image of the primary mirror inside the cryostat, and a 4K cold stop will be installed at this location to reduce stray light. The beam is converted by two cold (1K) high density polyethylene lenses, with a porous teflon AR coating, to a telecentric *f*/3.0 focus. A set of metal-mesh low-pass edge (LPE) filters and dielectric blocking filters are used to reduce the optical loading on the 300 mK stages, while a metal-mesh LPE combined with the feedhorn defines the bandpass.

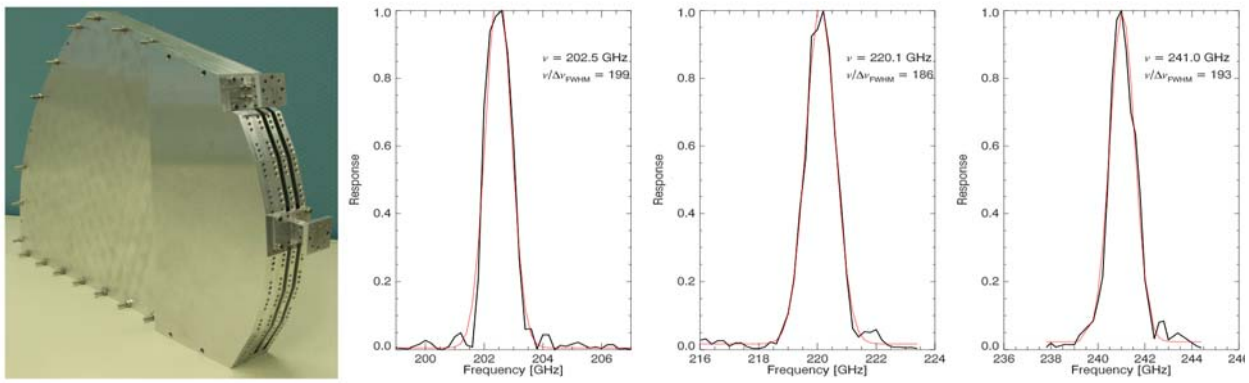

Figure 7. Waveguide spectrometer array prototyped based on this program. The prototype waveguide spectrometers demonstrate good spectral purity and realize the design spectral resolution.

The 1.0° linear field will be scanned along right ascension (RA) so that the scan rasters in azimuth at transit, aiding in sky subtraction. The orientation of the linear spectrometer array on the sky must be maintained as the parallactic angle of the field changes throughout the course of the night. The cryostat will therefore be mounted with an instrument rotator. As the target field rotates over time and the projection of the on-sky strip in horizontal (alt-az) coordinates changes, the cryostat will be rotated so as to keep the 16 beams oriented in the RA direction. The JCMT will then be scanned along the RA direction, requiring both azimuth and elevation

movement. The edge-field distortion in the reimaging optics limits the range of rotation about the transit angle, such that the outer few spectrometers are not used except within ±4 hours of transit. The effect is that, in a 9 hour observation, the net sensitivity is as if the full 16 beams were effectively used for 6.3 hours. Adding margin for bad weather and pointing, we conservatively assume 4 hours per night of useful on-source time on a single field. However we will either observe a second [CII] field or kSZ clusters while the primary field is transiting, to maximize the net observing efficiency.

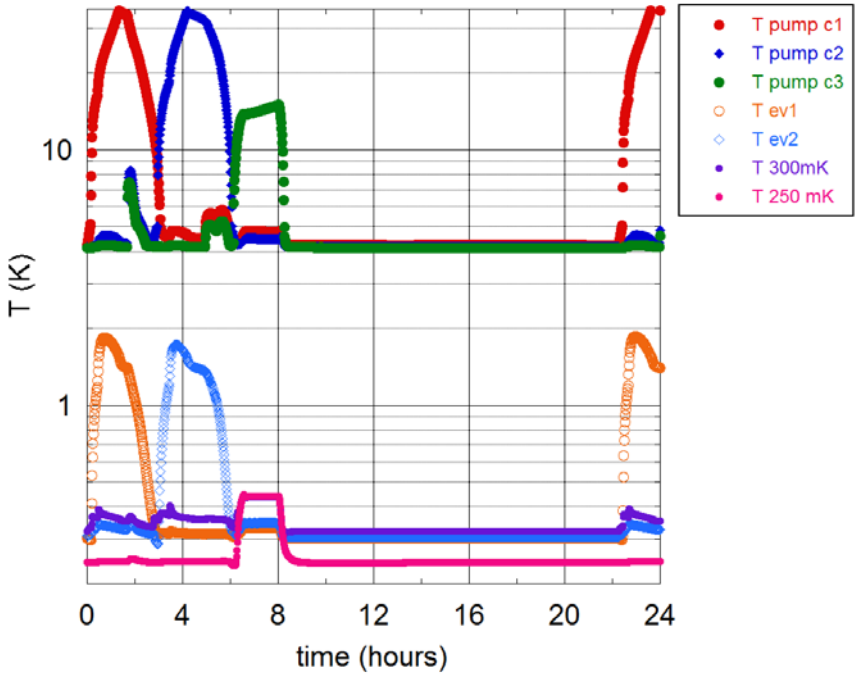

Figure 8: Measured thermal cycle of the TIME-*Pilot* multi-stage 3He cooling system. The full system (shown in the multi-panel figure 6) operates from a 4 K cooling stage provided by a pulse-tube cooler, avoiding the use of liquid cryogens at a remote mountain top site. The first stage is a closed ^{4}He loop that provides a continuous 1 K interface temperature. The next stage is a 450 mK intercept, provided by a double-stage 3He sorption system (C1/EV1 and C2/EV2 in the plot). The final stage is a 250 mK single-shot cooler. While the test shown here was run in a single-shot cycle, the 450 mK system can be run continuously, running one unit while the other condenses.

d. Leveraging an Existing Cryogenic System

TIME-*Pilot* will use an existing closed-cycle cryostat (Fig. 6) with a Cryomech PT-415 4K refrigerator that provides a base temperature < 4K, and includes two custom lower-temperature stages: a recirculating 4He system for 1K and a ^{3}He dual sorption system for 300mK. The integrated cryogenic system has been fully demonstrated (see Fig. 8) after adding a final ^{3}He stage to cool the gratings and detectors to a stable 250mK. The cryostat only requires modifications of the vacuum jacket as well as the existing 60 K, 4K, and 1K radiation shields. We will add a 300mK enclosure around the spectrometers and high-permeability magnetic shielding. The 4K stage provides the cold stop at a pupil, and the 1K stage will house the final polyethylene reimaging lens.

e. Spectroscopic Bolometer Arrays

TIME-*Pilot* will use arrays of silicon-nitride leg-isolated, superconducting transition edge sensor (TES) bolometers which are a natural extension of arrays we have fielded in many instruments. The 1931 detector count (1920 spectral + 11 150 GHz broadband channels) is less than the total number of detectors fielded in BICEP-2/Keck (3072 detectors), and it shares field-proven system-level approaches including: 1) an elemental titanium TES with TC = 450mK providing a steep transition and large loop gain, 2) a series aluminum (TC ~1K) TES that functions under

higher background for laboratory characterization, 3) NIST time-domain multiplexed SQUIDs, and 4) UBC multi-channel readout electronics (MCE).

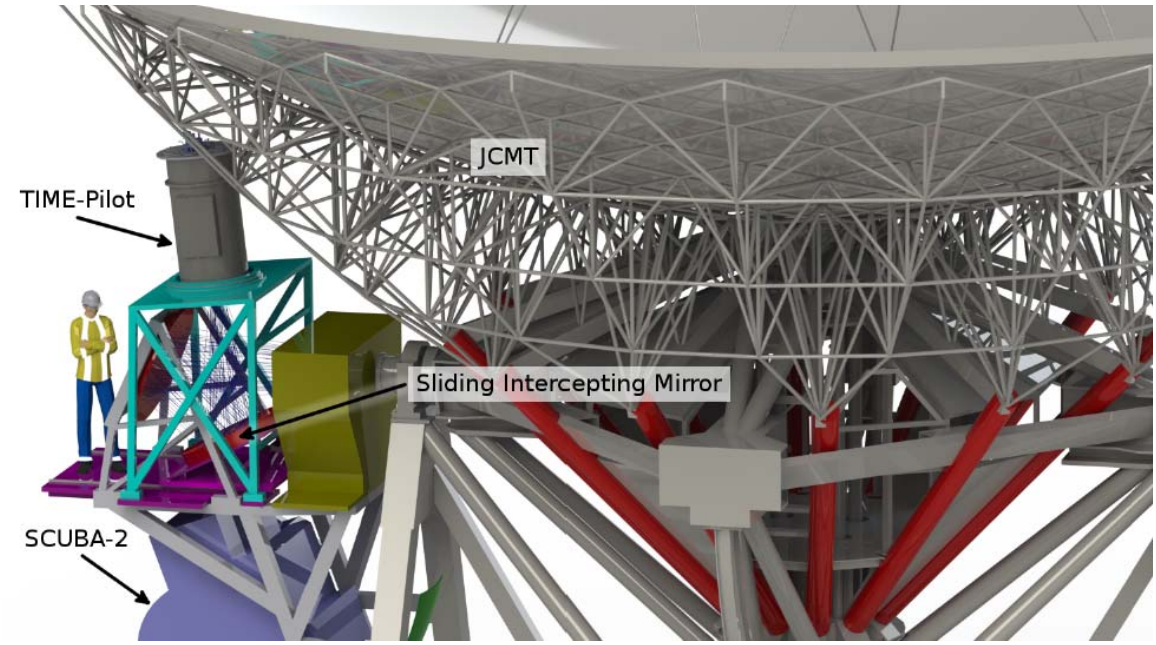

Figure 9. TIME-Pilot installed at the JCMT. The TIME-Pilot cryostat mounts above the platform that holds the current SCUBA-2 instrument and mirror. By adding one extra mirror, we intercept the beam headed toward SCUBA-2 and direct it upward to our instrument. The intercepting mirror will be on a platform that can slide the mirror away for quick switching back to normal SCUBA-2 observing.

Unlike antenna-fed CMB detectors, for TIME-*Pilot* we take the simpler approach of direct absorption on a micromesh (a.k.a. 'spider-web') absorber as was used in Z-Spec and Herschel SPIRE. With the narrow bandwidth on each detector, TIME-*Pilot* requires a noise equivalent power (NEP ~ 1×10^{-17} W $Hz^{-1/2}$) a bit higher than what has already been demonstrated in Z-Spec, while TES bolometers with much lower NEPs have been demonstrated in the lab.

We have developed a detector design with detailed noise and speed-of-response calculations for TIME-*Pilot* (Table 1). The 24 detector sub-arrays will be formed on sparsely-filled silicon dies, providing ample room for bolometer legs and wiring. Each 7 cm×3 cm die covers 8 stacked spectrometers in one of the grating output planes described above, and will carry 8x8=64 (low-frequency) or 8x12=96 (high-frequency) detectors. Photographs of a prototype TIME-*Pilot* sub-array die are shown in Figure 6. The die allows close packing in the spectral direction and features an integrated backshort formed by bulk etching of a double-SOI wafer. The pictured die is undergoing initial cryogenic dark testing now. Each pair of sub-array dies will be housed in a single assembly including a printed circuit board and a gold-plated aluminum housing which mounts to the spectrometer assembly (see Fig. 6). The array packages will be connected to two large multiplexing circuit boards via superconducting (aluminum on kapton) flex-cables similar to SPIDER CMB focal plane arrays.

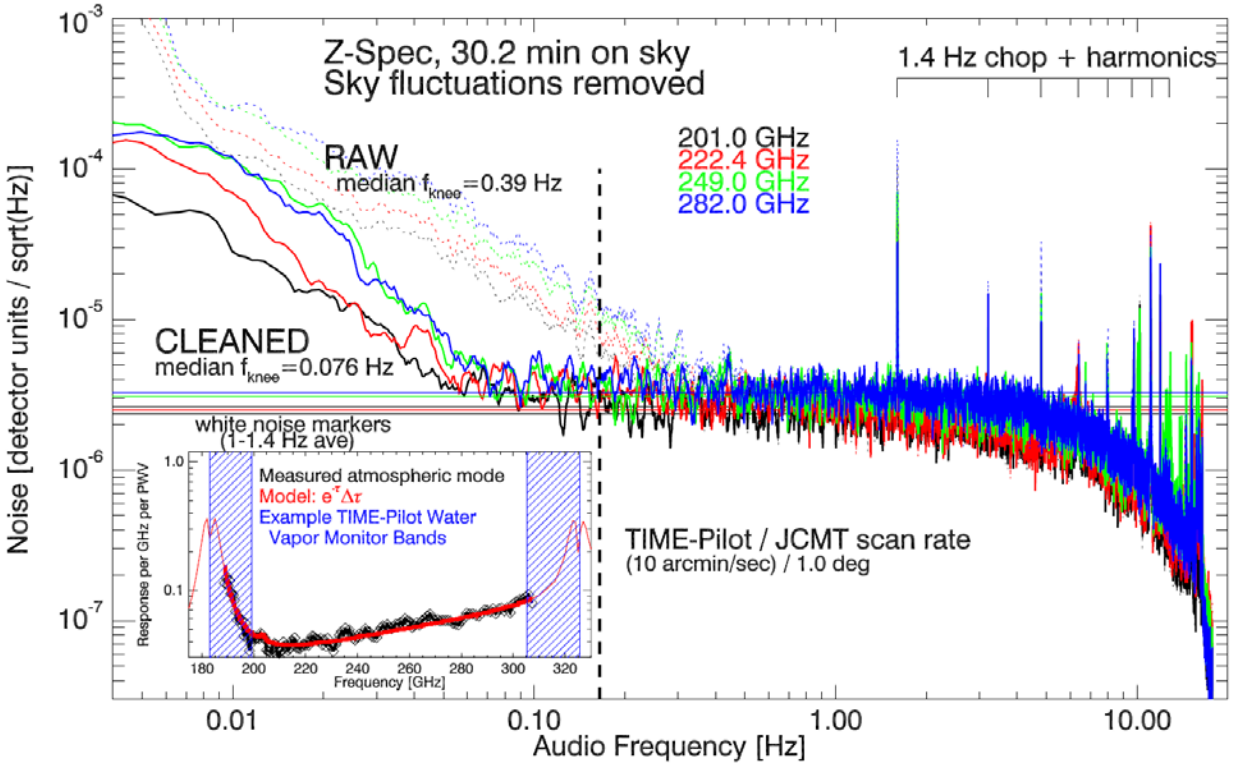

Figure 10: Sky noise measured in narrow spectral bands in a 30 minute staring observation by Z-Spec on the CSO. The low-frequency noise is largely common, due to fluctuations in precipitable water vapor (PWV) through the atmosphere. We have confirmed that it is readily removed by subtracting a variable-amplitude spectral mode which captures the fluctuations in the atmospheric emission. The resulting 1/f knee for a single channel is typically at ~ 0.07 Hz, well below the ~ 0.17 Hz scan frequency of the JCMT. The inset shows the measured spectral shape of the common mode, which matches well with a model for the derivative of the loading with the PWV. TIME-*Pilot* will extend Z-Spec's coverage (black points) into the blue shaded bands for improved atmospheric monitoring.

f. New Atmospheric Subtraction Method

To quantitatively predict the effect of atmospheric noise, we have generated simulations using a Kolmogorov turbulence (KT) model [71] which captures the temporal behavior of the atmospheric emission, including the effect of wind speed and direction, altitude of the turbulent layer, and the shape of the instrument beams as they passes through the atmosphere. The model assumes an atmospheric spectrum [85], calibrated by scaling to real Z-Spec observations shown in Fig. 10. We use this to generate simulated TIME-*Pilot* time streams from the KT model, and add uncorrelated instrumental white noise. We simulate our atmospheric noise reduction strategy by generating an atmospheric spectral template every scan by fitting a 2nd order polynomial to each scan for every channel. We then co-add the atmospheric monitor channels (183-199 GHz and 305-326 GHz), scale by the spectral template, and subtract this from the science channels (150 and 199-305 GHz). The monitor channels combined have > 3× the sensitivity to atmospheric emission as the science channels. Neglecting beam mismatching, we find a residual atmospheric component which is ~ 10% the nominal time stream noise. The sensitivity calculated in Fig. 3 assumes a loss in low spatial frequency information as a result of the polynomial template fitting.

This model is conservative, because we allow the spectrum of the atmosphere to vary on the timescale of a scan, at the price of increasing noise to derive a new spectral atmospheric template every scan. Further mitigation may be possible by adding another level of removal, spatial subtraction using correlated information over the linear array.

Papers / Technical Reports to date

S. Hailey-Dunsheath *et al*. 2015, "Low Noise Titanium Nitride KIDs for SuperSpec: A Millimeter-Wave On-Chip Spectrometer", JLTP, 112H.

A. Crites *et al*. 2014, "The TIME-*Pilot* Intensity Mapping Experiment", SPIE 9153E, 1WC.

B.D. Uzgil *et al*. 2014, "Measuring Galaxy Clustering and the Evolution of [CII] Mean Intensity with Far-IR Line Intensity Mapping during $0.5 < z < 1.5$", ApJ 793, 116U.

R. O'Brient *et al*. 2014, "Lithographed Spectrometers for Tomographic Line Mapping of the Epoch of Reionization", SPIE 9153E, 0FO.

S. Hailey-Dunsheath *et al*. 2014, "Status of SuperSpec: A Broadband, On-Chip Millimeter-Wave Spectrometer", SPIE 9153E, 0MH.

Z. Staniszewski *et al*. 2014, "The Tomographic Ionized-Carbon Mapping Experiment (TIME) CII Imaging Spectrometer", JLTP 176, 767S.

S. Hailey-Dunsheath *et al*. 2014, "Optical Measurements of SuperSpec: A Millimeter-Wave On-Chip Spectrometer", JLTP 176, 841H.

E. Shirokoff *et al*. 2014, "Design and Performance of SuperSpec: An On-Chip KID-Based mm-Wavelength Spectrometer", JLTP 176, 657S.

A. Pullen, O. Doré and J. Bock 2013, "Intensity Mapping Across Cosmic Times with the Lyman-Alpha Line", ApJ in press (arXiv 1309.2295).

M. B. Silva *et al*. 2013, "Intensity Mapping of Lyα Emission During the Epoch of Reionization", ApJ 763, 132.

Y. Gong, A. Cooray, M. Silva, M. G. Santos, J. Bock, C. M. Bradford, and M. Zemcov 2012, "Intensity Mapping of the [C II] Fine Structure Line during the Epoch of Reionization" ApJ, 745, 49.

Presentations / Conferences to date

"Statistical Measurements of Faint Reionizing Sources with Emission Line Intensity Mapping", M. Zemcov et al., The Reionization Epoch: New Insights and Future Prospects, Aspen, March 2016.

"Probing the Epoch of Reionization via CII Tomography with TIME-Pilot", C.M. Bradford *et al*., American Astronomical Society, Kissimmee, January 2016, 22742607B.

"Measuring Galaxy Clustering and the Evolution of [CII] Mean Intensity with Far-IR Line Intensity Mapping during 0.5 < z < 1.5", B. Uzgil *et al*., American Astronomical Society, Kissimmee, January 2016, 22733504U.

"Probing the Epoch of Reionization with CII Tomography: TIME-Pilot and Future Capabilities", A. Crites et al., U.S. Radio / Millimeter / Submillimeter Science Futures in the 2020s, Chicago, December 2015.

"Exploring the Epoch of Reionization with C+ Tomographic Mapping" J. Bock, *ASIAA Research Colloquium*, Taiwan, August 2013

"Intensity Mapping the Epoch of Reionization with C+ Line Emission" J. Bock, *Harvard ITC Luncheon*, April 2013.

"Probing the Epoch of Reionization with the Tomographic Ionized-carbon Mapping Experiment", J. Bock, *CCAT Workshop*, Boulder CO, August 2012.

V. Conclusions

We have developed a full scientific case for [CII] intensity mapping to study the epoch of reionization. We have developed a complete design for an instrument intended to make a first-light measurement of [CII] large-scale fluctuations, with the requisite sensitivity to detect the [CII] signal based on the amplitude predicted by a range of models. We feel a first-light measurement is appropriate due to test the astrophysical predictions, involving non-linear physics such as star formation and the production of light elements in the ISM. A first instrument is also necessary to demonstrate the real-world challenges for handling mode contamination from atmospheric noise and foreground removal. We have made significant progress in realizing TIME-Pilot with KISS funding, but have yet to secure the full funding needed to complete the instrument and carry out observations.